International Journal of Nanomedicine

Dovepress
open access to scientific and medical research

Open Access Full Text Article

ORIGINAL RESEARCH

Photothermal transforming agent and chemotherapeutic co-loaded electrospun nanofibers for tumor treatment

This article was published in the following Dove Press journal:
International Journal of Nanomedicine

Jiulong Zhao[1,*]
Yangbei Zhu[1,*]
Changqing Ye[2,*]
Ying Chen[2]
Shige Wang[2]
Duowu Zou[3]
Zhaoshen Li[1]

[1]Department of Gastroenterology, Changhai Hospital, Second Military Medical University, Shanghai 200433, People's Republic of China; [2]College of Science, University of Shanghai for Science and Technology, Shanghai 200093, People's Republic of China; [3]Department of Gastroenterology, Ruijin Hospital, School of Medicine, Shanghai Jiaotong University, Shanghai 200025, People's Republic of China

*These authors contributed equally to this work

Background: Photothermal and chemotherapy treatment has been frequently studied for cancer therapy; however, chemotherapy is equally toxic to both normal and cancer cells. The clinical application value of most kinds of photothermal transforming agents remains limited, due to their poor degradation and minimal accumulation in tumors.

Materials and methods: We reported the synthesis of photothermal transforming agents (MoS_2) and chemotherapeutic (doxorubicin, DOX) co-loaded electrospun nanofibers using blend electrospinning for the treatment of postoperative tumor recurrence.

Results: Under the irradiation of an 808 nm laser, the as-prepared chitosan/polyvinyl alcohol/MoS_2/DOX nanofibers showed an admirable photothermal conversion capability with a photothermal conversion efficiency of 23.2%. These composite nanofibers are in vitro and in vivo biocompatible. In addition, they could control the sustained release of DOX and the generated heat can sensitize the chemotherapeutic efficacy of DOX via enhancing its release rate. Their chemo-/photothermal combined therapy efficiency was systematically studied in vitro and in vivo. Instead of circulating with the body fluid, MoS_2 was trapped by the nanofibrous matrix in the tumor and so its tumor-killing ability was not compromised, thus rendering this composite nanofiber a promising alternative for future clinical translation within biomedical application fields.

Conclusion: Chitosan/polyvinyl alcohol/MoS_2/DOX nanofibers showed an excellent photothermal conversion capability with a photothermal conversion efficiency of 23.2% and can completely inhibit the postoperative tumor reoccurrence.

Keywords: electrospinning, chitosan, chemotherapy, photothermal tumor therapy, tumor

Introduction

Surgery, radiotherapy, and chemotherapy have played dominant roles in current cancer therapy; unfortunately, these cancer therapies, especially radiotherapy and chemotherapy, are equally toxic to both normal and cancer cells.[1,2] As a common chemotherapeutic drug, doxorubicin (DOX) has been frequently applied in tumor chemotherapy. However, apart from the high toxicity of DOX, its high in vivo permeability has caused an extremely low utilization ratio.[3,444] In order to solve the above problems, different kinds of drug carriers have been designed to simultaneously deliver DOX into the tumor to enhance drug usage and safety.

Another solution to realize safe and efficient cancer therapy is to explore minimally invasive therapy methods like photothermal therapy (PTT),[5] photodynamic therapy,[6,7] microwave ablation,[8] magnetic-hyperthermia regression,[9,10] gene

Correspondence: Zhaoshen Li
Department of Gastroenterology, Changhai Hospital, Second Military Medical University, No. 168 Changhai Road, Yangpu District, Shanghai 200433, People's Republic of China
Tel +86 213 116 1353
Email li.zhaoshen@hotmail.com

Duowu Zou
Department of Gastroenterology, Ruijin Hospital, School of Medicine, Shanghai Jiaotong University, No. 197 Ruijin Second Road, Huangpu District, Shanghai 200025, People's Republic of China
Tel +86 213 116 1355
Email zdw_pi@163.com

© 2019 Zhao et al. This work is published and licensed by Dove Medical Press Limited. The full terms of this license are available at https://www.dovepress.com/terms.php and incorporate the Creative Commons Attribution – Non Commercial (unported, v3.0) License (http://creativecommons.org/licenses/by-nc/3.0/). By accessing the work you hereby accept the Terms. Non-commercial uses of the work are permitted without any further permission from Dove Medical Press Limited, provided the work is properly attributed. For permission for commercial use of this work, please see paragraphs 4.2 and 5 of our Terms (https://www.dovepress.com/terms.php).

therapy,[11,12] and high-intensity focused ultrasound ablation.[13,14] Among them, PTT has been progressively unveiled in recent years for highly specific cancer therapy. The success of tumor PTT depends on the rational design of a biocompatible and multifunctional photothermal transforming agent (PTA) which can efficiently absorb and transform the near-infrared (NIR) laser into heat and burn out the tumor tissue.[15,16] In the past few decades, interest in the PTA design was continually aroused, and different kinds of inorganic PTAs such as noble metal,[17] transition metal sulfide,[18,19] transition metal carbide,[1,20] and organic PTAs including graphene oxide,[21] reduced graphene oxide,[22] and conductive polymers[23–26] have been continuously proposed. However, the clinical application value of most kinds of PTAs, especially inorganic PTAs, remains limited, probably owing to their poor degradation and minimal accumulation in tumors.

Bearing the aforementioned issues of chemotherapeutics and PTAs in mind, researchers have proposed various kinds of intelligent platforms including injectable hydrogel, oleosol, and polymeric implants for safely localized tumor treatments.[9,27] Electrospun polymer nanofibers, owing to their unique properties including high surface-to-volume ratio, tunable porosity, and ease of surface functionalization, have attracted high attention in a number of fields, such as filtration, textile manufacturing, catalysts, and pharmaceutics.[28–30] As a therapeutic carrier, nanofiber can improve the drug-loading capacity and effectively control drug release. Moreover, the nanofibrous matrix may exert a discernible impact on the safety of guest materials while not compromising their function.[27,31,32]

In a previous study, MoS_2 nanosheets and DOX-loaded poly(lactic-co-glycolic) acid (PLGA) nanofibers have been successfully prepared via directly electrospinning the mixture solution of PLGA, MoS_2, and DOX, for the efficient postoperative treatment of tumor in NIR I and NIR II biowindows.[27] However, due to the strong hydrophobicity of PLGA, PLGA/MoS_2/DOX nanofibers severely shrank after being implanted into the tumor site. As the N-deacetylated product of chitin, chitosan (CS) is the second-most abundant natural polysaccharide. CS has many unique properties like biocompatibility, biodegradability, antimicrobial activity, etc.[33] Nevertheless, due to the strong molecular interaction, CS has poor spinnability and is difficult to form into uniform nanofibers. In this study, we reported the design of an electrospun CS nanofiber-based carrier, using polyvinyl alcohol (PVA) as an adjuvant to enhance the spinnability of CS, to concurrently deliver PTA (MoS_2 nanosheets) and DOX for highly efficient multimodal postoperative tumor treatment. Using typical blending electrospinning, MoS_2 nanosheets and DOX were directly incorporated within the formed CS/PVA (CP) nanofibers. The multimodal postoperative tumor treatment efficiency of the as-prepared CP/MoS_2/DOX nanofibers was evaluated in vitro and in vivo. With tunable physicochemical properties such as the diameter and guest material-loading amount, the biocompatible nanofibers can control the release of DOX with a NIR laser-responsive manner and so retain MoS_2 nanosheets in tumors, thereby assuring highly efficient and safe postoperative tumor therapy.

Materials and methods

Electrospinning and crosslinking

The powder of PVA was dissolved in acetic acid aqueous solution (70 wt.%) to form a solution with concentration of 10 wt.% by magnetic stirring for 8 h at 80 °C. The powder of CS was dissolved in acetic acid aqueous solution (70 wt.%) at a concentration of 7 wt.%. The electrospinning solution was prepared by mixing the above two solutions as a CS/PVA solution (volume ratio 1:2). After this, MoS_2 nanosheets that were produced based on our previous report[34] were blended with CS/PVA solution for electrospinning. CP, CP/MoS_2, and CP/MoS_2/DOX nanofibers were fabricated via electrospinning under ambient conditions. Based on a previous study,[27] the concentration of MoS_2 nanosheets and DOX in the electrospinning solution was selected as 6 mg/mL and 10 mg/mL, respectively. The applied voltage was 20 kV, the collecting distance was 20 cm, and the solution feeding rate was 0.3 mL/h by homemade syringe pump. When the electrospinning process was finished, the nanofibrous mats were taken off the aluminum foil and dried in a vacuum oven.

The electrospun CP, CP/MoS_2, and CP/MoS_2/DOX nanofibers were crosslinked via a GA crosslinking method. The crosslinking solution was made up of 0.66 mL of GA, 15 mL of acetone, and 0.016 mL of concentrated hydrochloric acid. The nanofibers were immersed in the crosslinking solution for 1 h, and then taken out and washed with PBS three times to remove the unbound GA, acetone, and hydrochloric acid. After that, the nanofibrous mat was dried in a vacuum oven for 4 h, and underwent a subsequent heating treatment at 60 °C. The surface morphology of nanofibers was characterized using field-emission scanning transmission electron microscopy (FEI Magellan 400).

In vitro photothermal performance of CP/MoS_2 nanofibers

The in vitro photothermal performance of CP (control) and the CP/MoS_2 nanofibrous mat was systematically studied by altering the laser power density (0.3 W/cm^2, 0.5 W/cm^2, and 1 W/cm^2) and irradiation time (0–5 min). The temperature increase (△T) of irradiated nanofibers was monitored with a FLIR™ E60 infrared camera. The △T values of the CP/MoS_2 nanofibrous mat during 5 cycles of laser on/off irradiation (power density 1 W/cm^2, laser on 5 min, laser off 5 min in each circle) were recorded to explore the photothermal stability. The photothermal conversion efficiency (η) of the CP/MoS_2 nanofibers was quantified according to Korgel's report using equation(1):[35]

$$\eta = \frac{hs(T_{\max} - T_{surr}) - Q_{in,surr}}{I\left(1 - 10^{(-A(\lambda))}\right)} \quad (1)$$

In this equation, S stands for the surface area of the nanofibrous mat, and hS was calculated by measuring the natural cooling rate of the nanofibrous mat after switching off the light source. $T_{\max}$ represents the maximum temperature of the nanofibrous mat under NIR laser irradiation. T_{surr} represents the temperature of the surroundings. $Q_{in,\text{surr}}$ is the lost heat of nanofiber to the surroundings. I represents the laser power (mW). $A(\lambda)$ represents the absorbance of CP/MoS_2 nanofibers at a wavelength of 808 nm. More details to calculate η can be found in Supplementary materials.

Drug loading and in vitro drug release

To calculate the drug content of the CP/MoS_2/DOX nanofibrous mat, the absorbance of the crosslinking solution was recorded using an ultraviolet–visible (UV–Vis) spectrophotometer (Lambda 25; Perkin Elmer Inc., Waltham, MA, USA) and the concentration of DOX was calculated according to the standard curve. To study the in vitro drug release, 5 mg CP/MoS_2/DOX nanofibrous mat was put in a glass vial that contained 5 mL PBS with a pH of 7.4 (duplicate the normal physiological environment) or 5 mL sodium acetate–acetic acid buffer solution with a pH of 5.4 (duplicate the in vivo acidic circumstance of tumor). Then, the sample was incubated in a 37 °C or 54 °C vapor-bathing vibrator and vibrated at a speed of 90 rpm. At predetermined time points, 1.5 mL solution containing the released DOX was taken from each glass vial. After that, 1.5 mL corresponding fresh buffer solution was replenished. The absorbance of the released solution at 490 nm was recorded using a UV–Vis spectrophotometer (Lambda 25; Perkin Elmer) and the concentration of DOX was calculated according to the standard curve (pH 5.4 and 7.4, Figure S1).

Cell culture and in vitro biocompatibility

For cell culture, DMEM was added with 10% FBS, penicillin (100 units/mL), and streptomycin (100 μg/mL). Mouse fibroblast (L929) and human colorectal carcinoma (HT29) cells were cultured in a humidified incubator that was filled with 5% CO_2 at 37 °C. To study the in vitro biocompatibility, pristine CP and CP/MoS_2 nanofibers were deposited on a coverslip with diameter of 1 cm and then put in a 24-well plate and fixed with a homemade stainless ring. Cells directly cultured in cell culture plate were set as control. Before cell seeding, the nanofibrous mat was sterilized with 75% ethanol for 2 h. The L929 cell density was set at 5×10^4 cells/well when seeding the cells. After 24 h, 48 h, and 72 h of incubation, the viability of cells was studied using a cell counting kit-8 (CCK-8) and Dead/Live staining. For the cell morphology observation, the nanofibrous mat with cells was rinsed with PBS 3 times and fixed with 2.5 wt.% glutaraldehyde (4 °C, 2 h). Then, cells were dehydrated with ethanol and air dried. The cell morphology was observed using field-emission scanning transmission electron microscopy (FEI Magellan 400).

In vitro hemocompatibility

All animal experiments were performed under the guidance of Changhai Hospital, Second Military Medical University (Shanghai, People's Republic of China) and in accordance with the policies of the National Ministry of Health. Balb/c nude mice and Kunming (KM) mice were bought from Shanghai Slac Laboratory Animal Centre (Shanghai, People's Republic of China) and fed in Changhai Hospital, Second Military Medical University in accordance with the policies ethically and legally approved by the National Ministry of Health. The in vitro hemocompatibility of CP and CP/MoS_2 nanofibers was evaluated using mouse red blood cells (mRBCs). For this study, 0.9 mL mRBCs dispersed in PBS were mixed with 3.6 mL distilled water (served as positive control), 3.6 mL PBS (served as negative control), or 3.6 mL PBS containing 5 mg CP or CP/MoS_2 nanofibers. The above specimens were cultured at 37 °C for 2 h. After the incubation, the above mRBCs were centrifuged (10,000 rpm, 60 s) and the absorbance at 541 nm of supernatant was recorded using the Lambda 25 UV–Vis spectrophotometer. The absorbance value was recorded as D_t

(absorbance of supernatant from mRBCs treated with nanofibrous mat), D_{pc} (absorbance of supernatant from mRBCs treated with water), and D_{nc} (absorbance of supernatant from mRBCs treated with saline). The hemolytic percentage (HP) was quantified according to equation (2):[13]

$$HP(\%) = \frac{(D_t - D_{nc})}{(D_{pc} - D_{nc})} \times 100\% \quad (1)$$

In vivo hemocompatibility

The in vivo hemocompatibility of the nanofibrous mat was assessed by performing serum biochemistry and a routine blood parameters test. The routine blood parameters test was carried out using a Sysmex XS-800i automated hematology analyzer, and the serum biochemistry was performed using a DxC 800 automatic biochemical analyzer. The blood samples of these tests were obtained from KM mice that were hypodermically embedded with 5 mg CP/MoS_2 nanofibrous mat. Healthy KM mice were set as control. The time points of blood collection were day 7 and day 28 after nanofiber embedding. At each time point, 3 mice were anesthetized for heart puncturing to collect the blood. The analyzed parameters are listed in Supplemental materials.

Biodistribution of Mo ions and histocompatibility

The biodistribution of Mo ions was analyzed by selecting KM mice as a model. In brief, KM mice with subcutaneous CP/MoS_2 nanofibers (5 mg) embedded were euthanized after being fed for 7 days and 28 days. Major organs (heart, liver, spleen, lung, and kidney) were collected and digested using aqua regia to form a clear solution. The concentration of Mo ions in the above solution was quantified using an Agilent 700 Series ICP-OES. The in vivo histocompatibility of CP/MoS_2 nanofibers was evaluated with standard H&E staining. To this end, KM mice were hypodermically embedded with 5 mg CP (control) and CP/MoS_2 nanofibrous mat. Mice were euthanized after being fed for 7 days and 28 days to collect their major organs. The pictures of H&E staining were recorded using a Leica DM IL LED inverted phase contrast microscope. The body weight of KM mice was also weighed every 2 days during the feeding period.

In vitro tumor therapeutic efficiency

HT29 cells (5×10^4 cells/well) were seeded into a cell culture plate (24-well) and incubated in the cell incubator overnight. Then, 5 mg CP, CP/DOX, CP/MoS_2, or CP/MoS_2/DOX nanofibrous mat (sterilized with 75% alcohol for about 2 h and washed with PBS 3 times) was placed in the individual hole of a 24-well cell culture plate. After that, cells were irradiated with 808 nm for 5 min. The Dead/Live kit and CCK-8 were used to determine the metabolic activities of HT29 cells according to the instruction book. The absorbance collection was done using a microplate reader (MK3; Thermo Fisher Scientific, Waltham, MA, USA). The Dead/Live stained cell images were collected using the Leica DM IL LED inverted phase contrast microscope. The phase contrast microscopic and fluorescent photograph of HT 29 cells treated with CP/MoS_2/DOX nanofibers were recorded using an Olympus BX43 fluorescence microscope.

Postoperative tumor recurrence inhibition study

Approximately 10^7 HT29 cells were hypodermically injected into the back of Balb/c nude mice. A human colorectal carcinoma nodule with diameter of about 1 cm was formed after 3 weeks of feeding. Then, the tumor nodule was surgically excised. The postoperative tumor recurrence inhibition efficiencies of CP, CP/MoS_2, and CP/MoS_2/DOX nanofibrous mats were assessed as follows: 5 mg of CP, CP/MoS_2, or CP/MoS_2/DOX nanofibrous mats were embedded into tumor after surgery (group I, without any further treatment; group II, CP; group III, CP/MoS_2; group IV, CP/MoS_2/DOX; n=6). After sewing the wound, scars of mice were irradiated with the NIR laser for a period of 5 min (1 W/cm^2). The thermal images and temperature of laser-irradiated mice were recorded using the FLIR™ E60 camera. The tumor recurrence was evaluated by measuring the tumor volume and appearance was also recorded to assess the tumor postoperative treatment efficiency.

Statistical analysis

Statistical analysis was performed using one-way ANOVA. The significance level was 0.05, and the data were indicated for $p<0.05$, $p<0.01$, and $p<0.001$. The sample size was set as 3 (n=3) unless specified.

Results and discussions

Nanofiber preparation and characterization

In this study, the doped MoS_2 nanosheet with diameter of ~20 nm (Figure S2) was prepared according to our previous study.[34] MoS_2 nanosheets and DOX molecules were directly

dissolved in the electrospinning solution for the fabrication of composite nanofibers using blend electrospinning. During the electrospinning, the mixed solution was surface charged by the electric field, leading to a mutual charge repulsion force among polymer chains to counterbalance the surface tension. When the electric field intensity increased to a critical value, the repulsive electrical forces among polymer chains overcame the surface tension of polymers, making the polymers eject from the syringe needle and travel to the collecting plate. The solvent evaporated during the traveling process and the polymer fibers were formed randomly on the collecting plate. The surface morphologies of the resultant CP, CP/MoS_2, and CP/MoS_2/DOX nanofibers were observed using scanning electron microscopy (Figures 1 and 2). It was found that pristine CP nanofibers exhibit a typical 3-dimensional morphology with a smooth surface and diameter of 108.5±45.7 nm (Figure 1A). After adding MoS_2, the 3-dimensional morphology of CP nanofibers was not changed, but the diameter decreased to 83.3±37.4 nm (Figure 1B). When MoS_2 and DOX were added, the diameter of CP/MoS_2/DOX nanofibers increased to a size of 149.2±63.7 nm (Figure 1C). The change of nanofiber diameter may be attributed to the variation of electrospinning solution properties after adding MoS_2 and DOX.

Due to the hydrophilic nature of PVA, the composite CP nanofibers were dissolved upon contacting water. Therefore, in order to facilitate their biomedical application, GA was selected as a crosslinker to render the nanofibers with water stability. After crosslinking, the morphology of nanofibers did not change significantly; however, the diameter of the crosslinked CP, CP/MoS_2, and CP/MoS_2/DOX nanofibers increased to 117.4±42.4 nm (Figure 2A), 89.1±34.8 nm (Figure 2B), and 166.9±59.1 nm (Figure 2C), respectively. The increase of diameter is likely ascribed to swelling of the nanofibers during the crosslinking.

Photothermal performance

As a representative member of 2-dimensional transition metal sulfides, the MoS_2 nanosheet has been recognized as a typical biocompatible PTA. It is no wonder that doping of the MoS_2 nanosheet will render the CP/MoS_2 nanofibers with high photothermal conversion efficiency. To prove this hypothesis, the photothermal performance of CP/MoS_2 nanofibers was then performed with irradiation from the 808 nm NIR laser. The UV–Vis–NIR spectrum of CP/MoS_2 nanofibers was firstly studied, which found that CP/MoS_2 nanofibers showed an apparent light absorption in the test wavelength range (Figure S3A). Apparently, pure DOX has no classical light absorbance in the NIR region (Figure S3B); therefore, it can be inferred that adding DOX will not influence the light absorbance of CP/MoS2/DOX nanofibers. It was verified that the photothermal transformation outcome of CP/MoS_2 nanofibers was strongly related to the NIR laser power density and irradiation time (Figure 3). Under the laser power densities of 0.3, 0.5, and 1.0 W/cm^2, the △T values of CP/MoS_2 containing saline were determined as 13.2 °C, 21.5 °C, and 30.7 °C, respectively, after 5 min of laser irradiation (Figure 3A,B). However, without MoS_2, pure CP nanofiber showed no meaningful photothermal performance (Figure S4A,B), indicating that the photothermal conversion efficiency was solely originated from MoS_2 nanosheets. The corresponding infrared thermal images of CP/MoS_2 nanofibers under NIR irradiation were recorded using an infrared camera (FLIR™ E60) to further intuitively evaluate the photothermal performance. As shown in Figure 3B, the high-temperature area swiftly extended and reached whole coverage of the cell culture hole, further significantly suggesting the admirable in vitro photothermal transforming capability of CP/MoS_2 nanofibers. The photothermal conversion efficiency of CP/MoS_2 nanofibers was determined as 23.2% (Figure 3C, 1 W/cm^2, 5 min). Besides, CP/MoS_2 nanofibers were proved to be photothermally stable and the △T values did not show any apparent retrogress during the 5 cycles of continuous laser irradiation (△T=34.3 °C (cycle 1), 34.6 °C (cycle 2), 34.2 °C (cycle 3), 34.8 °C (cycle 4), and 34.7 °C (cycle 5), power density 1 W/cm^2; Figure 3D). CP/MoS_2 nanofibers with such an apparent photothermal efficiency and stability are anticipated to act as an encouraging PTA to find universal applications for PTT cancer treatment.

DOX loading and release from CP/MoS_2/DOX nanofibers

As a drug reservoir, the CP/MoS_2 nanofibers can load and control the release of DOX. The concentration of DOX released to the crosslinking solution was calculated to be 0.74 mg/mL. Therefore, the drug content of the CP/MoS_2/DOX nanofibrous mat was computed as 3.68%. The absorbance of the crosslinking solution was recorded using a UV–Vis spectrophotometer (Lambda 25; Perkin Elmer) to calculate the DOX concentration according to the standard curve. It was found that the DOX release was characterized with a pH/temperature dual-modal responsive and sustainable manner (Figure 4). The initial release rate was slightly fast, likely

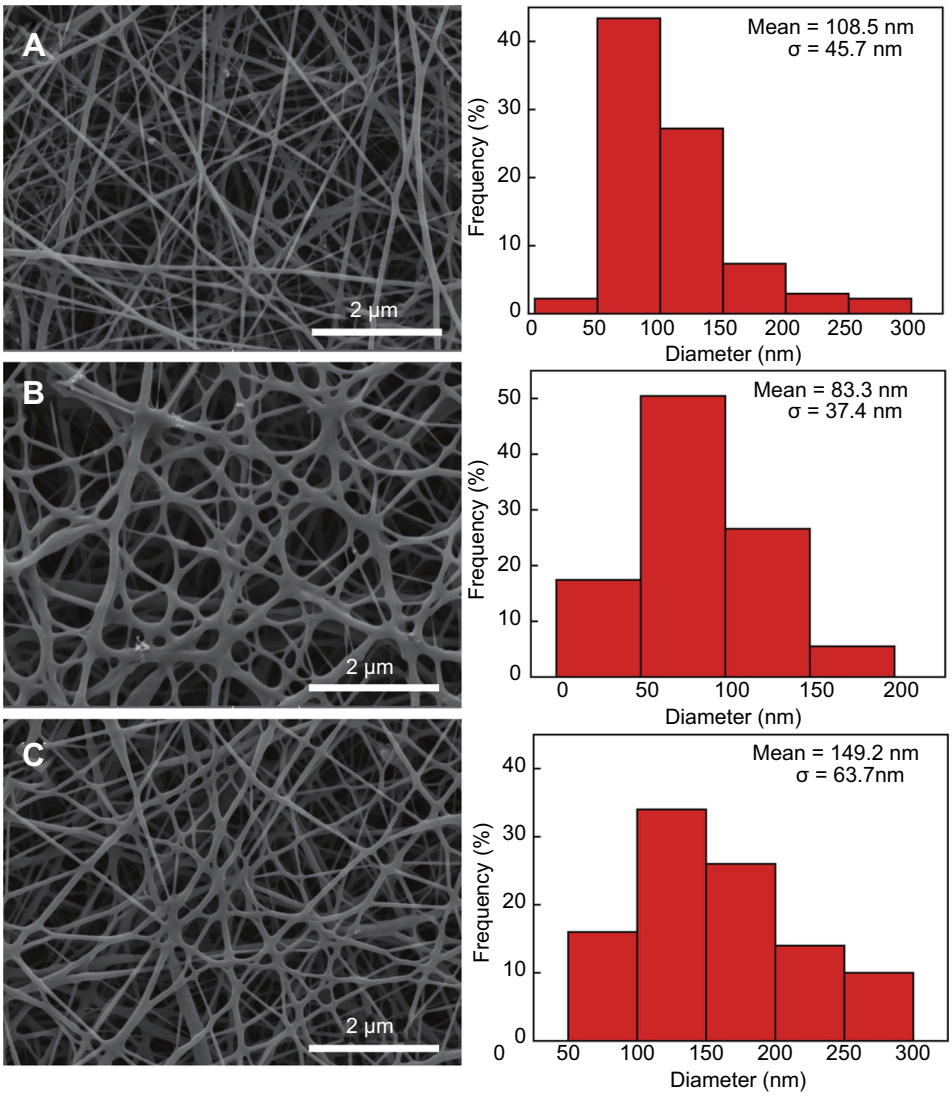

Figure 1 Characterization of nanofibers. (A) Scanning electron microscopy pictures and diameter distribution of (**A**) chitosan/polyvinyl alcohol (CP), (**B**) CP/MoS_2, and (**C**) CP/MoS_2/doxorubicin nanofibers.

owing to the hydrophilic surface of CP nanofibers. The cumulative release amount reached a plateau after 6 h at all of the tested pHs and temperatures. In addition, the release rate can be promoted by the increasing temperature and decreasing pH, likely due to the increased DOX solubility in mild acidic conditions and high temperature. For example, the total release amount was 11.0±1.7% under physiological conditions (pH 7.4, T=37 °C), but it sharply increased to 65.8±2.5% under tumor PTT conditions (pH 5.4, T=54 °C). Such a pH and temperature dual-modal responsive drug release profile renders the nanofibers with the ability to augment the tumor therapy, since the generated heat under NIR laser irradiation not only can kill tumor cells by hyperthermia, but can also sensitize the chemotherapeutic efficacy of DOX via enhancing its release rate. Moreover, this drug loading is anticipated to be universally extended to the loading of many categories of other drugs with a high loading capacity, providing the drug was soluble in electrospinning solution.

In vitro cytocompatibility

We then studied the cytocompatibility, which is the basic prerequisite for safe biomedical application of the nanofibrous mat, using CCK-8 and Dead/Live staining (Figure 5 and Figure S5). It was found that the viability of L929 cells on CP and CP/MoS_2 nanofibers was higher than 95% (CP: 98.4%; CP/MoS_2: 98.1%), and showed no detectable difference when compared with healthy L929 cells (p>0.05) after 24 h of culture (Figure S5A). The cell viability of healthy cells cultured on CP and CP/MoS_2 nanofibers was then qualitatively evaluated by performing

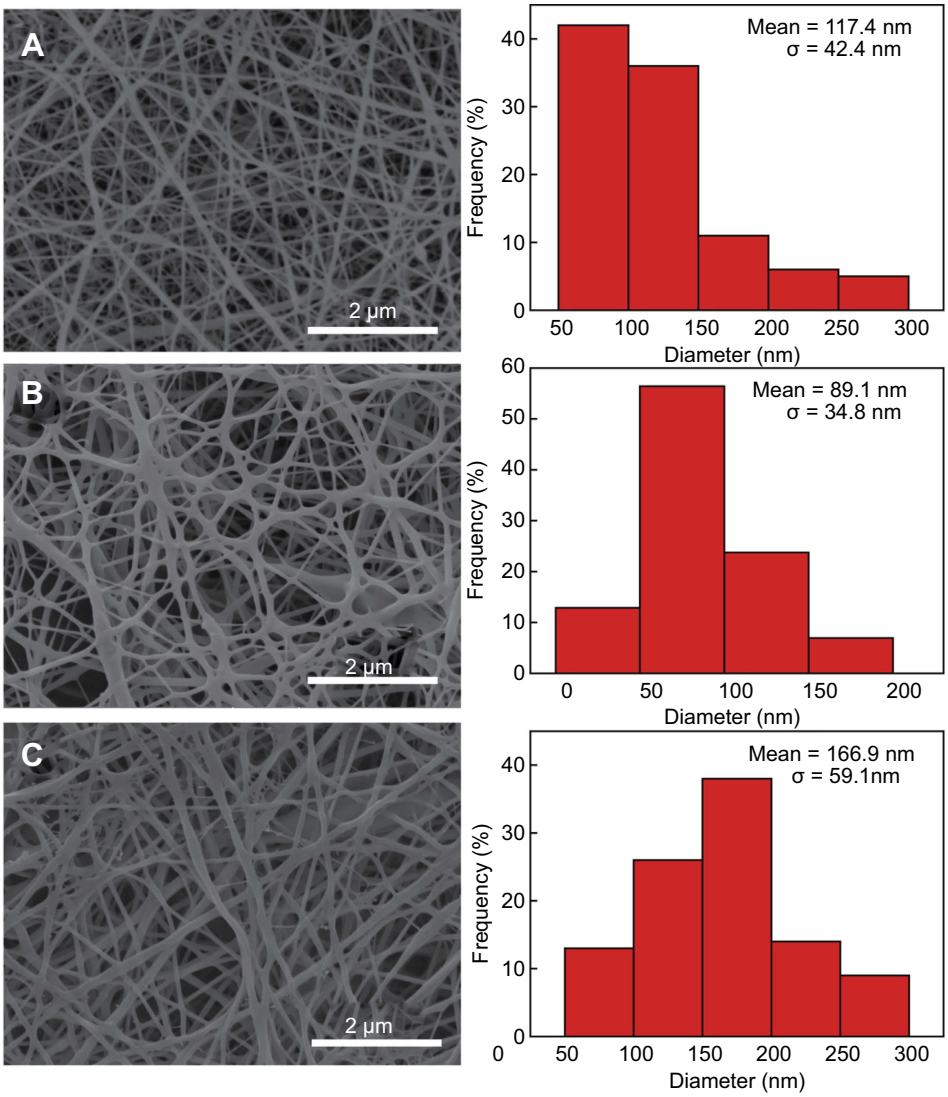

Figure 2 Characterization of crosslinked nanofibers. (**A**) Scanning electron microscopy pictures and diameter distribution of GA-crosslinked (**A**) chitosan/polyvinyl alcohol (CP), (**B**) CP/MoS_2, and (**C**) CP/MoS_2/doxorubicin nanofibers.

Dead/Live staining, which can stain live and dead cells green and red, respectively. In accordance with the CCK-8, almost all cells turned green during the Dead/Live staining, confirming the insignificant cytotoxicity of the composite nanofibers (Figure S5B–D).

To further evaluate the biocompatibility of the nanofibrous carrier, the longer-term proliferation level of L929 cells cultured on nanofibers was monitored by performing CCK-8 and cell morphology observation. L929 cells proliferated smoothly on both the CP and CP/MoS_2 nanofibers, and their proliferation viability was comparable with cells cultured onto the cell culture plate at different time points (Figure 5). The morphology of L929 cells cultured onto CP and CP/MoS_2 nanofibrous mats for 24 h, 48 h, and 72 h was observed by scanning electron microscopy (Figure 5C). Qualitatively corroborating with the CCK-8 assay results (Figure 5A), it was found that both CP and CP/MoS_2 nanofibers can support the migration, adhesion, and proliferation of L929 cells onto the fiber surface, and a typical three-dimensional cell-matrix structure was formed at all of the tested time points, further suggesting the excellent biocompatibility of the CP and CP/MoS_2 nanofibers.

In vitro hemocompatibility

Red blood cells play a dominant role in the transportation of oxygen and nutrients. Therefore, the hemocompatibility of CP/MoS_2 nanofibers necessarily needs to be verified. The hemocompatibility assessment was initially performed by performing in vitro hemolysis, where the mRBCs were

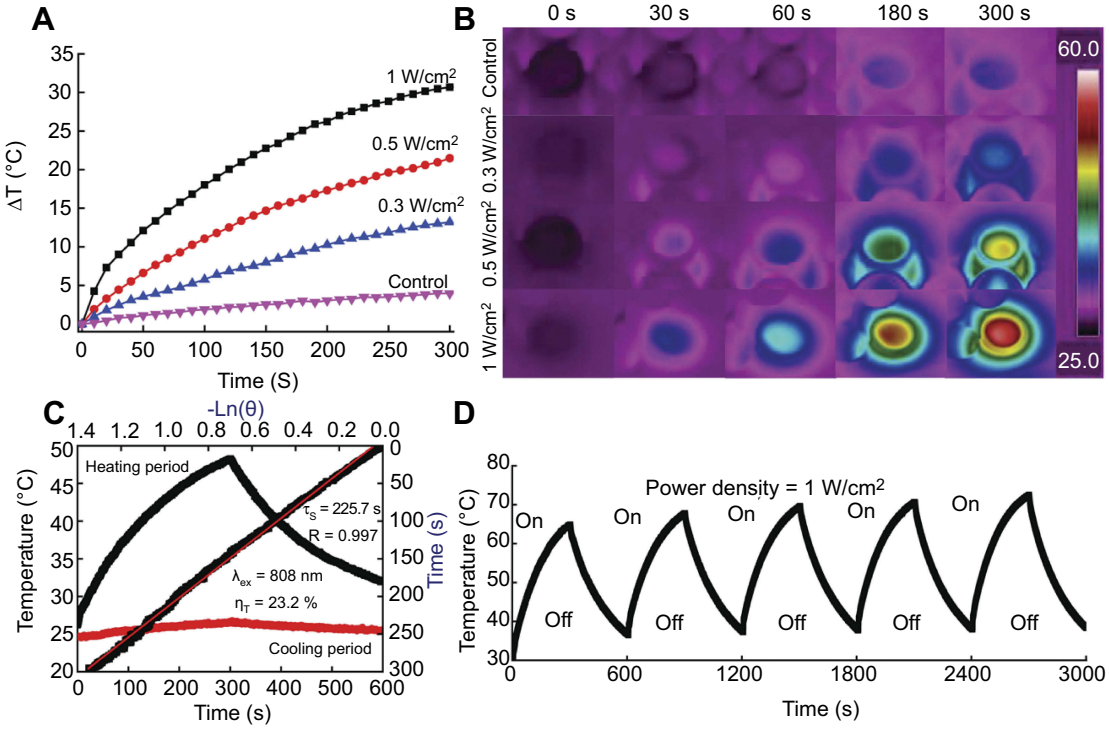

Figure 3 In vitro photothermal performance of nanofibers. (**A**) Power density-related temperature changes (△T) of CP/MoS_2 nanofibers during 300 s of irradiation by 808 nm near-infrared laser. (**B**) Thermal images of CP/MoS_2 nanofibrous mat at different time points corresponding to (A). (**C**) Steady state heating curve and heat transfer time constant of CP/MoS_2 nanofibers (power density 1 W/cm^2, 5 min; R=0.997, τ_s=225.7 s). (**D**) 808 nm laser-induced recycling photothermal ability of CP/MoS_2 nanofibers.
Abbreviation: CP, chitosan/polyvinyl alcohol.

individually treated with saline (negative control), water (positive control), CP, and CP/MoS_2 nanofibers. The structural integrity of mRBCs can be completely preserved and the hemolysis ratio was defined as 0 in saline, while the structural integrity of mRBCs can be totally destroyed in water and the hemolysis ratio was defined as 100%. As shown in Figure 5B, the hemolysis ratio of CP and CP/MoS_2 nanofibers was calculated as 1.8±0.4% and 2.8±0.8% after 2 h of incubation, respectively. In accord with the hemolysis ratio, mRBCs can be readily separated from the solution upon incubation with saline, CP, and CP/MoS_2 nanofibers, further indicating that the impact of CP and CP/MoS_2 nanofibers on the structural integrity of mRBCs is negligible.[3636]

In vivo biocompatibility

Before moving to the in vivo tumor therapy study, the biocompatibility of CP/MoS_2 was further explored using healthy KM mice. After embedding the subcutaneous nanofibers, all of the KM mice gained weight progressively and showed negligible difference compared with healthy KM mice, preliminarily confirming that the CP/MoS_2 nanofibers do not cause obvious side effects on the physical condition of KM mice (Figure 6A). To prove that the CP/MoS_2 nanofibrous carrier can ensure highly efficient tumor therapy by retaining the great mass of MoS_2 nanosheets in tumor sites, the in vivo release of MoS_2 nanosheets from the polymeric matrix was analyzed by studying the biodistribution of Mo ions in major organs of KM mice using ICP, at 7 days and 28 days after subcutaneous nanofiber embedding (Figure 6C). It was discovered that the Mo ion accumulation in the heart, liver, spleen, lung, and kidney was limited. For example, the content of Mo in the spleen was about 4.7±1.0 μg/g and 3.5±0.3 μg/g after 7 days and 28 days of feeding; this content only accounted for about 0.2% of the total dose of MoS_2 in the composite nanofibrous mats, indicating that the vast majority of MoS_2 nanosheets were entrapped within tumor and thereby their potential health threats to living body can be eliminated. It is worth noting that the laser irradiation will not lead to obvious influence on the biodistribution of Mo ions, because MoS_2 nanosheets[34] and CP/MoS_2 nanofibers have been proved photothermal stable under 5 cycles of laser irradiation.

The in vivo compatibility of CP/MoS_2 nanofibers was further studied by performing in vivo hemocompatibility using the serum biochemistry and routine blood test on day 7 and day 28 after subcutaneous embedding. Similar to healthy mice, blood routine parameters and serum

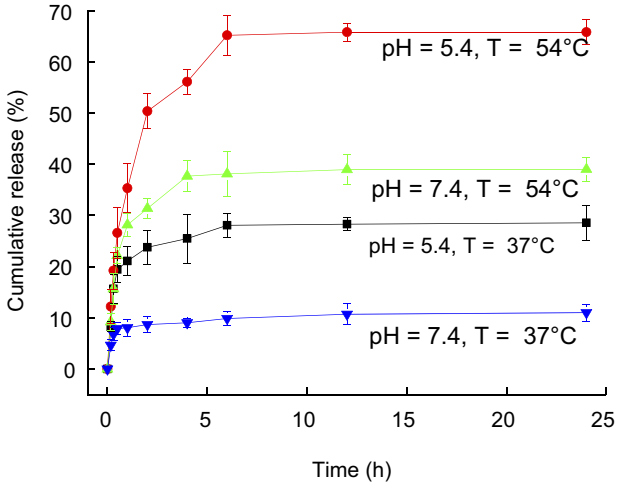

Figure 4 Doxorubicin release from CP/MoS_2 nanofibrous mat at different pH with (T=54 °C) or without (T=37 °C) near-infrared irradiation (1 W/cm^2).
Abbreviation: CP, chitosan/polyvinyl alcohol.

biochemistry parameters of experimental animals fluctuate in the normal range (Figure 6B and Figure S7), implying healthy physiological functions of the main organs and blood of CP/MoS_2 nanofiber-treated mice. Then, the above KM mice were euthanized to harvest their major organs for standard H&E staining (Figure 6D). Consistent with the body weight and in vivo hemocompatibility assay, the main organs of the tested KM mice showed no obvious pathological abnormity after 7 days and 28 days of feeding. The in vitro and in vivo analysis data confirm the excellent hemocompatibility of the as-synthesized composite nanofibers, providing more evidence for the feasibility and practicality of safe in vivo applications of CP/MoS_2 nanofibers. Together with the above proved photothermal conversation capacity, such CP/MoS_2/DOX nanofibers are anticipated to have different applications for highly efficient and secure tumor treatments.

In vitro tumor therapeutic efficiency

After proving the excellent photothermal efficiency, photothermal stability, controlled drug release, and biocompatible

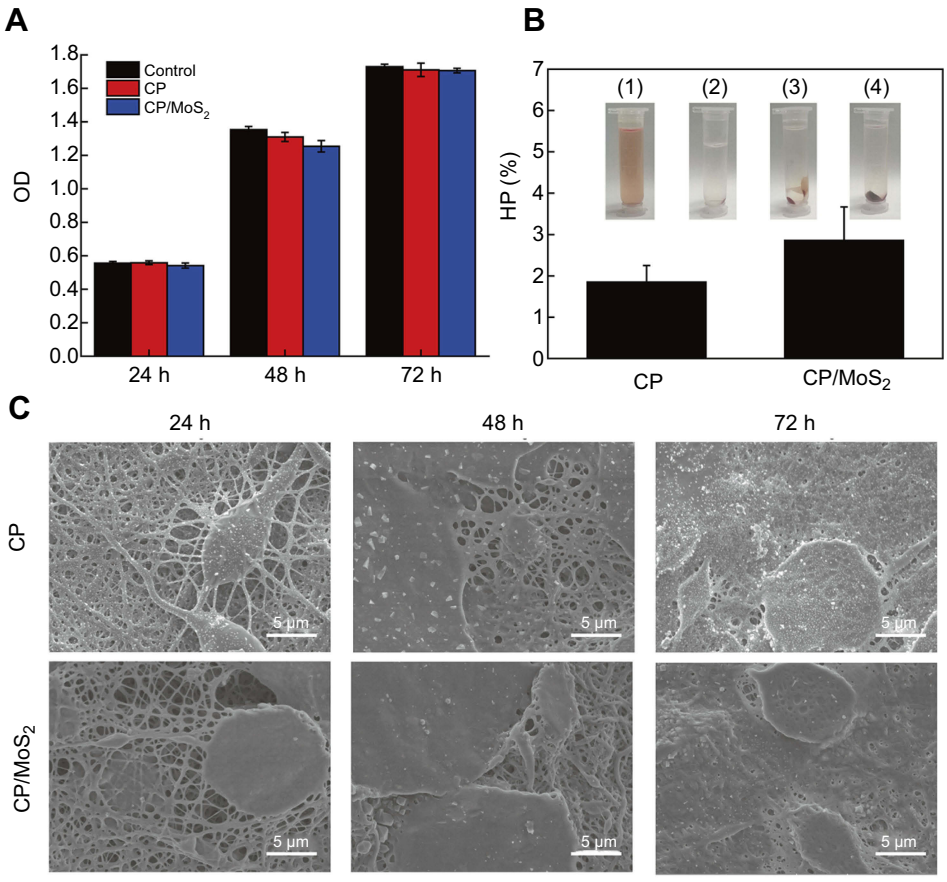

Figure 5 In vitro cytocompatibility and hemocompatibility assays of crosslinked nanofibers. (**A**) Proliferation viability of L929 cells on cell culture plate, CP, and CP/MoS_2 nanofibers after 24 h, 48 h, and 72 h of culture. (**B**) Hemolytic percentage (HP) of mRBCs treated with CP and CP/MoS_2 nanofibers. Inset images are the centrifuged mRBCs after 2 h of incubation with (1) water, (2) saline, (3) CP, and (4) CP/MoS_2 nanofibers. (**C**) Scanning electron microscopy micrographs of L929 cells cultured on CP and CP/MoS_2 nanofibers after 24 h, 48 h, and 72 h culture.
Abbreviations: CP, chitosan/polyvinyl alcohol; OD, optical density; HP, hemolytic percentage; mRBC, mouse red blood cell.

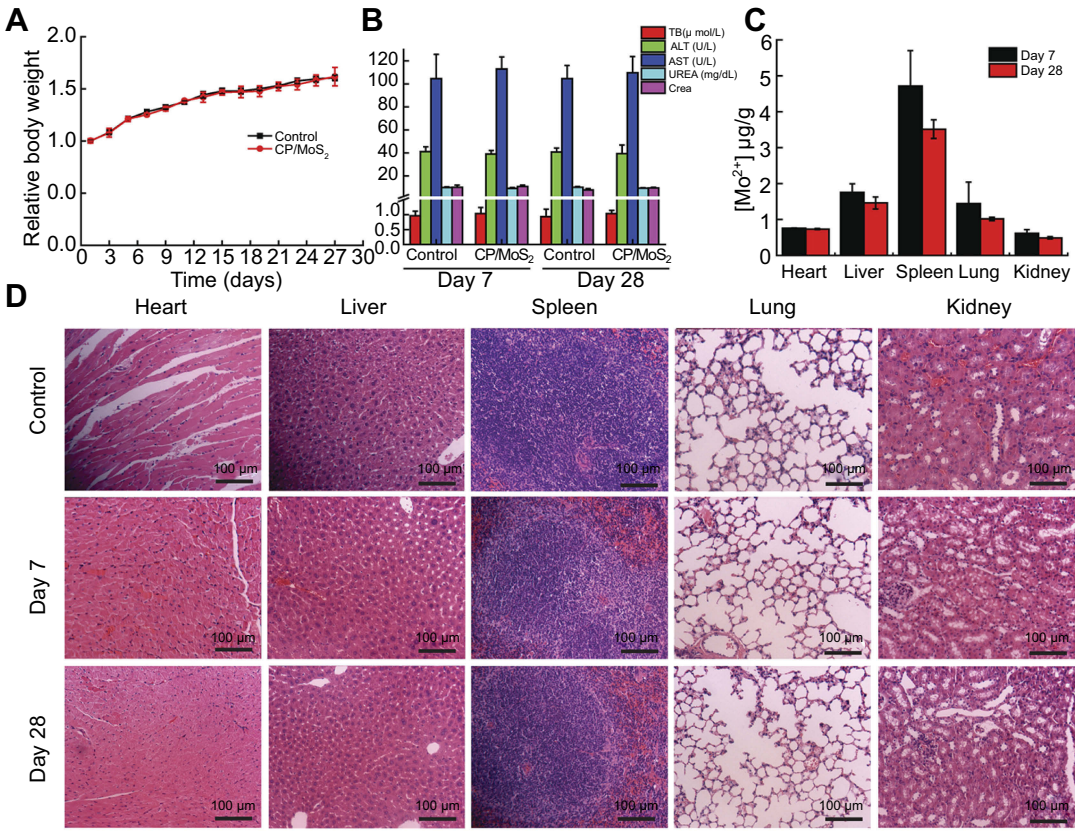

Figure 6 In vivo biocompatibility assays of crosslinked nanofibers. (**A**) Body weight evolution curves of healthy KM mice and KM mice with subcutaneous CP/MoS_2 nanofiber embedding. (**B**) Blood biochemistry parameter. (**C**) Biodistribution of Mo element. (**D**) H&E staining images of KM mice with subcutaneous CP/MoS_2 nanofiber embedding.
Abbreviations: ALT, alanine aminotransferase; AST, aspartate aminotransferase; CP, chitosan/polyvinyl alcohol; KM, Kunming; TB, total bilirubin.

nature of the electrospun CP/MoS_2 nanofibers, we then systematically studied the combined chemotherapy and PTT efficiency in vitro using HT29 cells and in vivo using the HT29 tumor-bearing nude mice. As shown in Figure S6, obvious red color and red fluorescence can be detected from the phase contrast microscopic and fluorescent photograph of HT29 cells treated with CP/MoS_2/DOX nanofibers (Figure S6C,D). However, no visible and fluorescent red signal was observed from HT29 cells treated with saline (Figure S6A,B), inferring that DOX release from CP/MoS_2/DOX nanofibers can be efficiently internalized by HT29 cells. The viability of HT29 cells cultured onto CP/DOX nanofibers decreased to 46.2±6.2% after 24 h of incubation (Figure 7A). After being exposed under the 808 nm laser for 5 min, the viability of HT29 cells onto CP/MoS_2 nanofibers significantly decreased to 12.7±0.8% (Figure 7A), resulting from the photothermal effect of the doped MoS_2 nanosheets. Under the coexistence of the photothermal effect of MoS_2 and the chemotherapeutic efficiency of DOX, CP/MoS_2/DOX nanofibers can completely suppress the malignant proliferation of tumor cells, and the viability of HT29 cells cultured therein for 24 h sharply decreased to 2.1±0.8% after being irradiated with the 808 nm laser for 5 min. To further prove the in vitro photothermal and chemotherapy tumor therapy capacity of CP/MoS_2 nanofibers, HT29 cells after the above treatments were further stained using the Dead/Live kit. Without DOX and MoS_2, pure CP nanofibers showed no anti-tumor efficiency; therefore, almost all of the cells cultured with CP nanofibers were stained green. In accordance with the CCK-8 assay, a section of HT29 cells were stained red after single photothermal or chemotherapy, and the red-stained cell portion of CP/DOX was smaller than that of CP/MoS_2+NIR. Oppositely, nearly all of HT29 cells were killed and stained red (Figure 7B–E) when adopting the combined therapy, confirming the combined tumor photothermal and chemotherapy efficiency of CP/MoS_2/DOX nanofibers.

Postoperative tumor recurrence inhibition study

Encouraged by the obvious in vitro tumor recurrence inhibition efficiency, CP/MoS_2/DOX nanofibers were

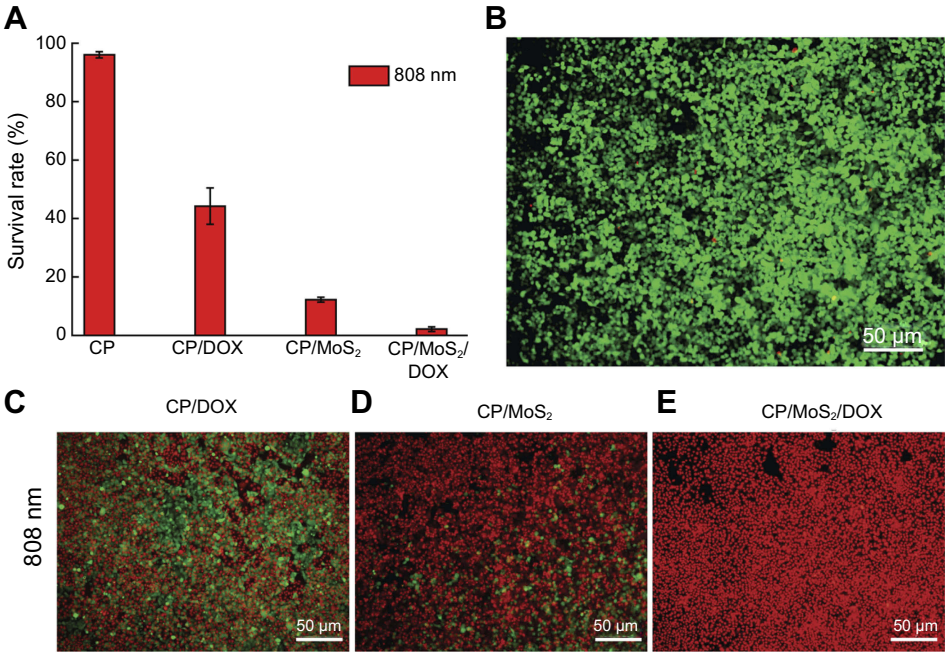

Figure 7 In vitro therapeutic efficacy of crosslinked nanofibers. (**A**) In vitro photothermal therapy and chemotherapy of CP, CP/DOX, and CP/MoS_2 and CP/MoS_2/DOX nanofibers. (**B–E**) Dead/Live staining of HT29 cells treated with (**B**) control, (**C**) CP/DOX+NIR, (**D**) CP/MoS_2+NIR, and (**E**) CP/MoS_2/DOX+NIR.
Abbreviations: CP, chitosan/polyvinyl alcohol; DOX, doxorubicin; NIR, near infrared.

hypodermically embedded within the tumor site that was excised to see their in vivo tumor postoperative recurrence inhibition ability. The in vivo photothermal conversion performance of CP/MoS_2/DOX nanofibers was firstly monitored, which revealed that the in vitro photothermal conversion ability of CP/MoS_2 nanofibers was well inherited after subcutaneous embedding within the tumor site. Upon 30 s of laser irradiation (1 W/cm^2), a swift tumor temperature augmentation of 8.1 °C was found, and the maximum △T can reach 31.8 °C during 5 min of continuous laser irradiation (Figure 8A,B). Moreover, the introduction of DOX exerted no apparent influence on the in vivo photothermal conversion of CP/MoS_2 nanofibers (Figure 8A,B). However, the maximum △T values of untreated mice and mice treated with pristine CP nanofibers were merely 6.5 °C and 7.7 °C (Figure 8A and Figure S2). The in vivo infrared thermal images further proved the remarkable photothermal transform capacity of CP/MoS_2/DOX nanofibers (Figure 8B). CP/MoS_2/DOX nanofibers with excellent in vivo photothermal conversion and controllable DOX release induce a satisfactory therapeutic result. Due to the photothermal and chemotherapy efficiencies of CP/MoS_2/DOX, the postoperative tumor recurrence of mice with CP/MoS_2/DOX embedding was totally prohibited and the scar was completely healed after 28 days of feeding (Figure 8C,D). In sharp contrast, owing to the incomplete clearance of tumor cells, untreated mice and mice treated with pristine CP nanofibers endured a natural tumor recurrence and the tumor volume expanded to 12.3 ±2.3 cm^3 and 10.3±2.4 cm^3 after 28 days of feeding, respectively (Figure 8C). Notably, although the photothermal conversion capability (η=23.2%) of CP/MoS_2 nanofibers is lower than previously reported MoS_2-containing nanofibers,[27] the NIR-induced hyperthermia of CP/MoS_2 nanofibers can still efficiently restrain the tumor recurrence in this study. It is no wonder that total inhibition of tumor recurrence can also be realized under a lower power density (lower than 1 W/cm^2) since a combined photothermal and chemotherapy capacity of CP/MoS_2/DOX nanofibers exists.

Conclusion

In summary, the primary aim of this nanofiber design is to deliver a sufficient amount of PTAs and chemotherapeutics to tumors. To this end, smooth and uniform MoS_2 and DOX co-loaded composite nanofibers were fabricated using blend electrospinning. After loading MoS_2 nanosheets, the as-prepared CP/MoS_2/DOX nanofibers showed an excellent photothermal conversion capability (η=23.2%). In addition, the composite nanofibers could control the sustained release of DOX. It was revealed that the designed composite nanofibers possess excellent in

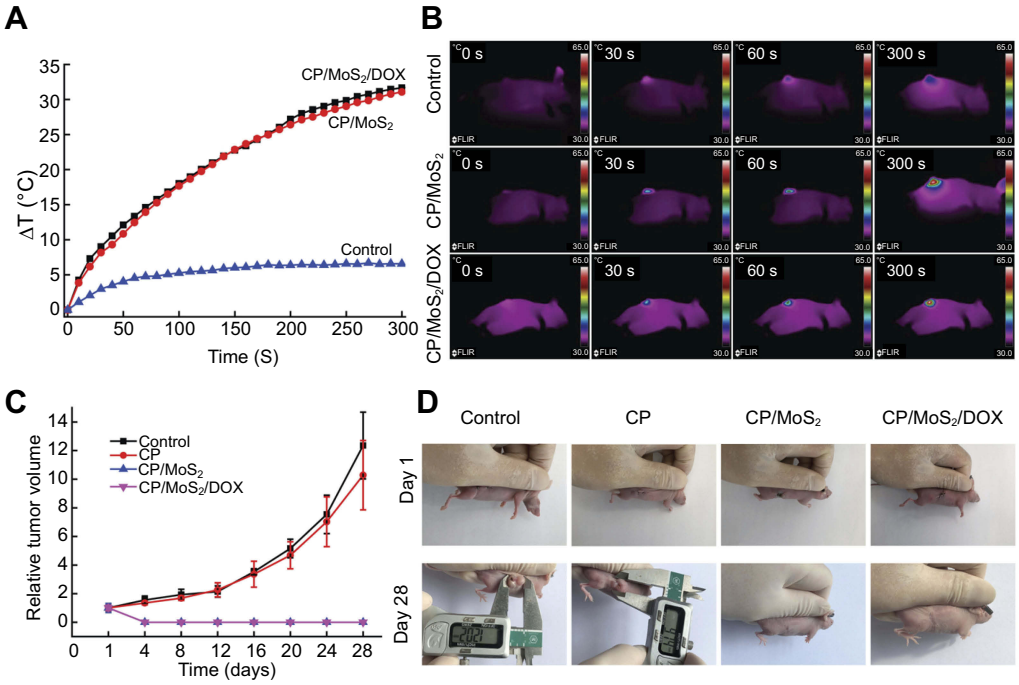

Figure 8 In vivo therapeutic efficacy of crosslinked nanofibers. (**A**) In vivo photothermal performance of CP/MoS_2 nanofibrous mat (control: mice without treatment). (**B**) In vivo thermal images of mice receiving different treatments as noted. (**C**) Postoperative tumor volume of mice receiving different treatments as noted. (**D**) Representative photographs of HT29 tumor-bearing mice corresponding to (C).
Abbreviations: △T, temperature increase; CP, chitosan/polyvinyl alcohol; DOX, doxorubicin.

vitro and in vivo biocompatibility. Moreover, the generated heat under NIR laser irradiation can sensitize the chemotherapeutic efficacy of DOX via controlling its release rate. The combined chemo-/photo thermal therapy efficiency of the composite nanofibers was systematically studied in vitro using HT29 cells and in vivo using HT29 tumor-bearing nude mice. The results prove that the postoperative tumor reoccurrence was completely prohibited owing to the combined tumor photothermal and chemotherapy efficiency of CP/MoS_2/DOX nanofibers. Instead of circulating with the body fluid, MoS_2 was confined to the tumor site by the nanofiber matrix while the tumor-killing ability was not compromised, therefore rendering the concept to design composite nanofibers a promising clinical translation in biomedical application fields.

Acknowledgments

The authors are grateful for the financial support from the National Natural Science Foundation of China (Grant Nos 51702214, 81470800, and 81670485), and Shanghai Sailing Program (17YF1412600) supported by the Shanghai Committee of Science and Technology.

Disclosure

The authors report no conflicts of interest in this work.

References

1. Lin H, Gao S, Dai C, Chen Y, Shi J. A two-dimensional biodegradable niobium carbide (MXene) for photothermal tumor eradication in NIR-I and NIR-II biowindows. *J Am Chem Soc*. 2017;139(45):16235–16247. doi:10.1021/jacs.7b07818
2. Wang S, Zhao J, Yang H, et al. Bottom-up synthesis of WS_2 nanosheets with synchronous surface modification for imaging guided tumor regression. *Acta Biomater*. 2017;58:442–454. doi:10.1016/j.actbio.2017.06.014
3. Zhitnyak I, Bychkov I, Sukhorukova IV, et al. Effect of BN nanoparticles loaded with doxorubicin on tumor cells with multiple drug resistance. *ACS Appl Mater Interfaces*. 2017;9(38). doi:10.1021/acsami.7b08713
4. Ma Y, Liang X, Tong S, Bao G, Ren Q, Dai Z. Gold nanoshell nanomicelles for potential magnetic resonance imaging, light-triggered drug release, and photothermal therapy. *Adv Funct Mater*. 2013;23(7):815–822. doi:10.1002/adfm.v23.7
5. Yang H, Zhao J, Wu C, Ye C, Zou D, Wang S. Facile synthesis of colloidal stable MoS_2 nanoparticles for combined tumor therapy. *Chem Eng J*. 2018;351:548–558. doi:10.1016/j.cej.2018.06.100
6. Lan G, Ni K, Xu R, et al. Nanoscale metal-organic layers for deeply penetrating X-ray-induced photodynamic therapy. *Angew Chem Int Edit*. 2017;56(40):12102–12106. doi:10.1002/anie.201704828
7. Rong P, Kai Y, Avinash S, et al. Photosensitizer loaded nano-graphene for multimodality imaging guided tumor photodynamic therapy. *Theranostics*. 2014;4(3):229–239.

8. Ma L, Zhou Y, Zhu Y, et al. 3D printed personalized titanium plates improve clinical outcome in microwave ablation of bone tumors around the knee. *Sci Rep*. 2017;7(1):7626.
9. Chen Y, Jiang L, Wang R, et al. Injectable smart phase-transformation implants for highly efficient in vivo magnetic-hyperthermia regression of tumors. *Adv Mater*. 2014;26(44):7468–7473.
10. Sonvico F, Mornet S, Vasseur S, et al. Folate-conjugated iron oxide nanoparticles for solid tumor targeting as potential specific magnetic hyperthermia mediators: synthesis, physicochemical characterization, and in vitro experiments. *Bioconjugate Chem*. 2005;16(5):1181–1188. doi:10.1021/bc050050z
11. Li C, Hu J, Li W, Song G, Shen J. Combined bortezomib-based chemotherapy and p53 gene therapy using hollow mesoporous silica nanospheres for p53 mutant non-small cell lung cancer treatment. *Biomater Sci*. 2016;5(1):77–88. doi:10.1039/c6bm00449k
12. Shen J, Sheng X, Chang Z, et al. Iron metabolism regulates p53 signaling through direct heme-p53 interaction and modulation of p53 localization, stability, and function. *Cell Rep*. 2014;7(1):180–193. doi:10.1016/j.celrep.2014.02.042
13. Wang S, Zhao J, Hu F, et al. Phase-changeable and bubble-releasing implants for highly efficient HIFU-responsive tumor surgery and chemotherapy. *J Mat Chem B*. 2016;4(46):7368–7378. doi:10.1039/C6TB01861K
14. Chen Y, Chen H, Sun Y, et al. Multifunctional mesoporous composite nanocapsules for highly efficient MRI-guided high-intensity focused ultrasound cancer surgery. *Angew Chem*. 2011;123(52):12713–12717. doi:10.1002/ange.201106180
15. Yang B, Chen Y, Shi J. Material chemistry of two-dimensional inorganic nanosheets in cancer theranostics. *Chem*. 2018;4(6):1284–1313. doi:10.1016/j.chempr.2018.02.012
16. Wu C, Wang S, Zhao J, et al. Biodegradable Fe(III)@WS_2-PVP nanocapsules for redoxReaction and TME-enhanced nanocatalytic, photothermal,and chemotherapy. *Adv Funct Mater*. 2019;201901722. doi:10.1002/adfm.201901722
17. Tang S, Chen M, Zheng N. Sub-10-nm Pd nanosheets with renal clearance for efficient near-infrared photothermal cancer therapy. *Small*. 2014;10(15):3139–3144. doi:10.1002/smll.201303631
18. Chen L, Zhou X, Nie W, et al. Marriage of albumin-gadolinium complexes and MoS_2 nanoflakes as cancer theranostics for dual-modality magnetic resonance/photoacoustic imaging and photothermal therapy. *ACS Appl Mater Interfaces*. 2017;9(21):17786–17798. doi:10.1021/acsami.7b04488
19. Chhowalla M, Liu Z, Zhang H. Two-dimensional transition metal dichalcogenide (TMD) nanosheets. *Chem Soc Rev*. 2015;44(9):2584–2586. doi:10.1039/c5cs90037a
20. Lin H, Wang YW, Gao SS, Chen Y, Shi JL. Theranostic 2D tantalum carbide (MXene). *Adv Mater*. 2018;30(4):1703284. doi:10.1002/adma.v30.4
21. Gulzar A, Xu J, Yang D, et al. Nano-graphene oxide-UCNP-Ce6 covalently constructed nanocomposites for NIR-mediated bioimaging and PTT/PDT combinatorial therapy. *Dalton T*. 2018;47(11):3931–3939. doi:10.1039/C7DT04141A
22. Shao L, Zhang R, Lu J, Zhao C, Deng X, Wu Y. Mesoporous silica coated polydopamine functionalized reduced graphene oxide for synergistic targeted chemo-photothermal therapy. *ACS Appl Mater Inter*. 2017;9(2):1226–1236. doi:10.1021/acsami.6b11209
23. Liu H, Li W, Cao Y, Guo Y, Kang Y. Theranostic nanoplatform based on polypyrrole nanoparticles for photoacoustic imaging and photothermal therapy. *J Nanopart Res*. 2018;20(3):57. doi:10.1007/s11051-018-4157-y
24. Zhang D, Wu M, Zeng Y, et al. Chlorin e6 conjugated poly(dopamine) nanospheres as PDT/PTT dual-modal therapeutic agents for enhanced cancer therapy. *ACS Appl Mater Interfaces*. 2015;7(15):8176–8187. doi:10.1021/acsami.5b01027
25. Wang J, Guo Y, Hu J, et al. Development of multifunctional polydopamine nanoparticles as a theranostic nanoplatform against cancer cells. *Langmuir*. 2018;34:9516–9524. doi:10.1021/acs.langmuir.8b01769
26. Li W, Wang X, Wang J, et al. Enhanced photoacoustic and photothermal effect of functionalized polypyrrole nanoparticles for near-infrared theranostic treatment of tumor. *Biomacromolecules*. 2019;20:401–411. doi:10.1021/acs.biomac.8b01453
27. Ye C, Zhao J, Zheng Y, et al. Preparation of poly(lactic-co-glycolic acid)-based composite microfibers for postoperative treatment of tumor in NIR I and NIR II biowindows. *Macromol Biosci*. 2018;1800206. doi10.1002/mabi.201800206
28. Wang S, Hu F, Li J, et al. Design of electrospun nanofibrous mats for osteogenic differentiation of mesenchymal stem cells. *Nanomed-Nanotechnol*. 2018;14:2505–2520. doi:10.1016/j.nano.2016.12.024
29. Chen M, Li YF, Besenbacher F. Electrospun nanofibers-mediated on-demand drug release. *Adv Healthc Mater*. 2014;3(11):1721–1732. doi:10.1002/adhm.201400166
30. Yang YY, Liu ZP, Yu DG, Wang K, Liu P, Chen X. Colon-specific pulsatile drug release provided by electrospun shellac nanocoating on hydrophilic amorphous composites. *Int J Nanomed*. 2018;13:2395–2404. doi:10.2147/IJN.S154849
31. Wang K, Liu XK, Chen XH, Yu DG, Yang YY, Liu P. Electrospun hydrophilic janus nanocomposites for the rapid onset of therapeutic action of helicid. *ACS Appl Mater Interfaces*. 2018;10(3):2859–2867. doi:10.1021/acsami.7b17663
32. Liu X, Shao W, Luo M, Bian J, Yu DG. Electrospun blank nanocoating for improved sustained release profiles from medicated gliadin nanofibers. *Nanomaterials*. 2018;8(4):184. doi:10.3390/nano8040184
33. Liao H, Qi R, Shen M, et al. Improved cellular response on multi-walled carbon nanotube-incorporated electrospun polyvinyl alcohol/chitosan nanofibrous scaffolds. *Colloid Surface-B*. 2011;84(2):528–535. doi:10.1016/j.colsurfb.2011.02.010
34. Zhao J, Zhou C, Mao L, et al. Bottom-up synthesis of ultra-small molybdenum disulfide-polyvinylpyrrolidone nanosheets for imaging-guided tumor regression. *Oncotarget*. 2017;8(63):106707–106720. doi:10.18632/oncotarget.22477
35. Tian Q, Hu J, Zhu Y, et al. Sub-10 nm Fe_3O_4@ $Cu_{2-x}S$ core-shell nanoparticles for dual-modal imaging and photothermal therapy. *J Am Chem Soc*. 2013;135(23):8571–8577. doi:10.1021/ja4013497
36. Guo B, Zhao J, Wu C, et al. One-pot synthesis of polypyrrole nanoparticles with tunable photothermalconversion and drug loading capacity. *Colloid Surface-B*. 2019;177:346–355. doi:10.1016/j.colsurfb.2019.02.016

Supplementary materials

Calculation of the photothermal conversion efficiency and supplementary figures.

Materials

Chitosan (medium molecular weight, degree of deacetylation>90%), glutaraldehyde (50% aqueous solution), acetic acid, polyvinyl alcohol (high molecular weight, 88% hydrolyzed), PBS, cell counting kit-8 (CCK-8), and Dead/Live kit were purchased from Sigma Chemicals (Perth, Australia). DOX was commercially purchased from Beijing Huafeng Pharmaceutical Co., Ltd. (People's Republic of China). Mouse fibroblast (L929) and human colorectal carcinoma (HT29) cell lines were commercially purchased from the Institute of Biochemistry and Cell Biology (Chinese Academy of Science, Shanghai, People's Republic of China). DMEM, FBS, penicillin, and streptomycin were products of Gibco (Thermo Fisher Scientific, Waltham, MA, USA). Water with resistivity higher than 18.2 MΩ.cm was purified using a Milli-Q Plus 185 water purification system (EMD Millipore, Billerica, MA, USA).

Calculation of the photothermal conversion efficiency

The formulas related to the calculation of efficiency are listed as follows:

(1) The product of heat transfer coefficient (h) and the surface area of the container (*S*) is:

$$hS = \frac{m \bullet C_{H_2O}}{\tau_s}$$

where m and C_{H2O} are the mass and specific heat capacity of the CP/MoS_2 nanofibers, and τ_s is the time constant.

(2) τ_s can be calculated by the following formula:

$$t = -\tau s \ln\left(\frac{T - Tsurr}{T\max - Tsurr}\right)$$

where t (s) is the time of the cooling process, T(°C) is the real-time temperature of t, T_{max} (°C) is the highest temperature of the sample, and T_{surr} (°C) is the temperature of the surroundings.

(3) The baseline energy input without a sample (Q_{Dis}) independently measured at about 808 nm was 17.12 mW.

(4) The absorbance of the sample ($A(\lambda)$) at the excitation wavelength of 808 nm was measured as about 4.1.

The studied routine blood test and biochemistry test parameters

The analyzed routine blood parameters include red blood cells (RBC), white blood cells (WBC), hemoglobin (HGB), hematocrit (HCT), mean corpuscular volume (MCV), mean corpuscular hemoglobin (MCH), mean corpuscular hemoglobin concentration (MCHC), platelet (PLT), and red cell distribution width (RDW). The studied biochemistry parameters include aspartate aminotransferase (AST), alanine aminotransferase (ALT), total bilirubin (TBIL), and carbamide (CAR).

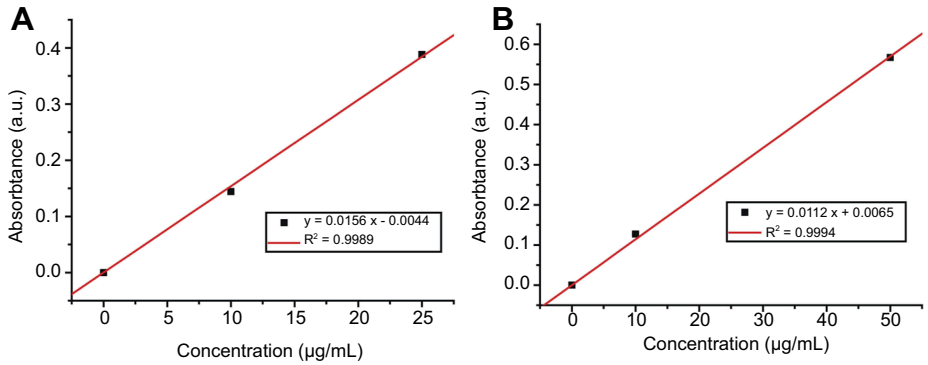

Figure S1 The standard curve of doxorubicin at (**A**) pH 5.4 and (**B**) pH 7.4.

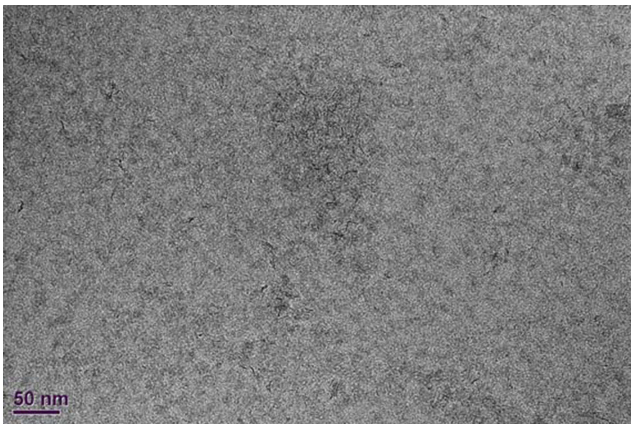

Figure S2 Transmission electron microsopy image of MoS_2 nanosheets.

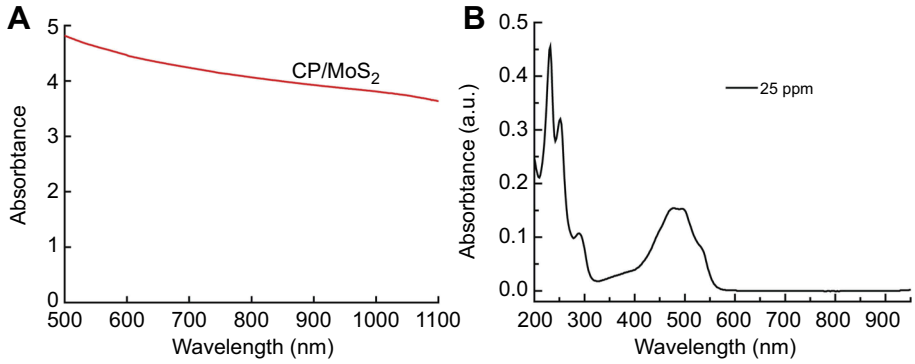

Figure S3 Ultraviolet–visible–near-infrared spectrum of **(A)** CP/MoS_2 nanofibers and **(B)** DOX.
Abbreviation: CP, chitosan/polyvinyl alcohol.

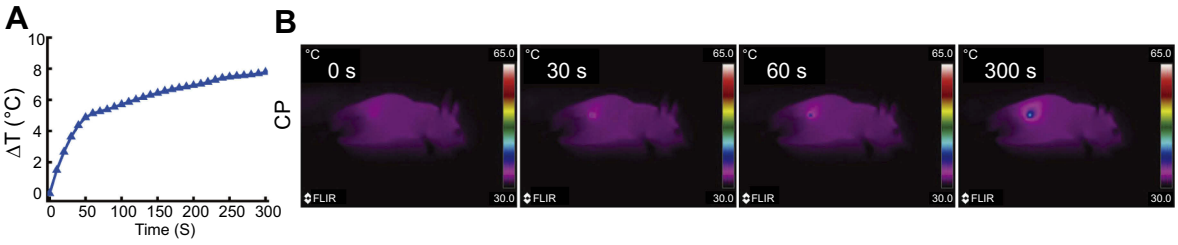

Figure S4 (**A**) In vivo photothermal performance of CP nanofibrous mat. (**B**) In vivo thermal images of mice corresponding to (A).
Abbreviations: △T, temperature increase; CP, chitosan/polyvinyl alcohol.

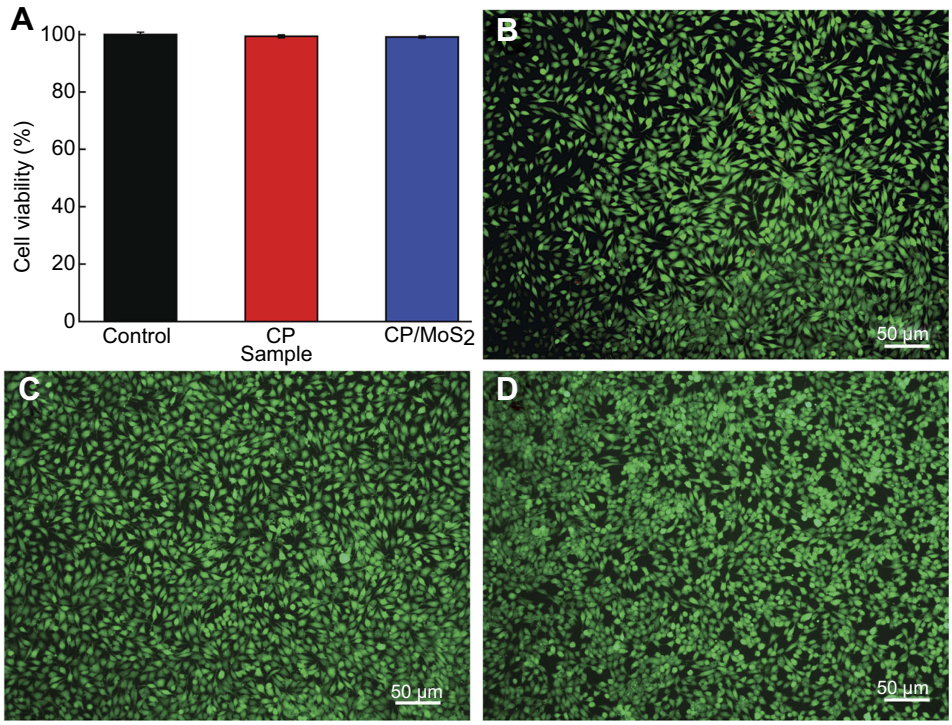

Figure S5 (**A**) The viability of L929 cells after incubation with saline, CP, and CP/MoS_2 nanofibers. (**B–D**) Dead/Live phase contrast images of L929 cells after treatment with (**B**) saline, (**C**) CP, and (**D**) CP/MoS_2 nanofibers for 24 h.
Abbreviation: CP, chitosan/polyvinyl alcohol.

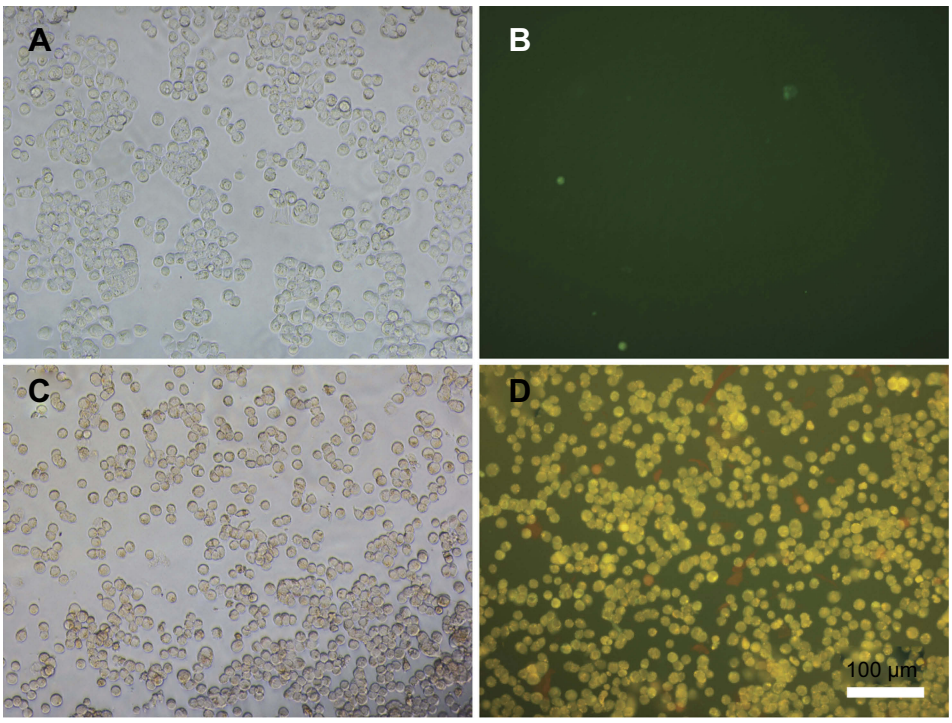

Figure S6 Phase contrast microscopic (**A, C**) and fluorescent (**B, D**) photographs of HT29 cells treated with saline (**A, B**) and CP/MoS_2/DOX nanofibers (**C, D**).
Abbreviation: CP, chitosan/polyvinyl alcohol.

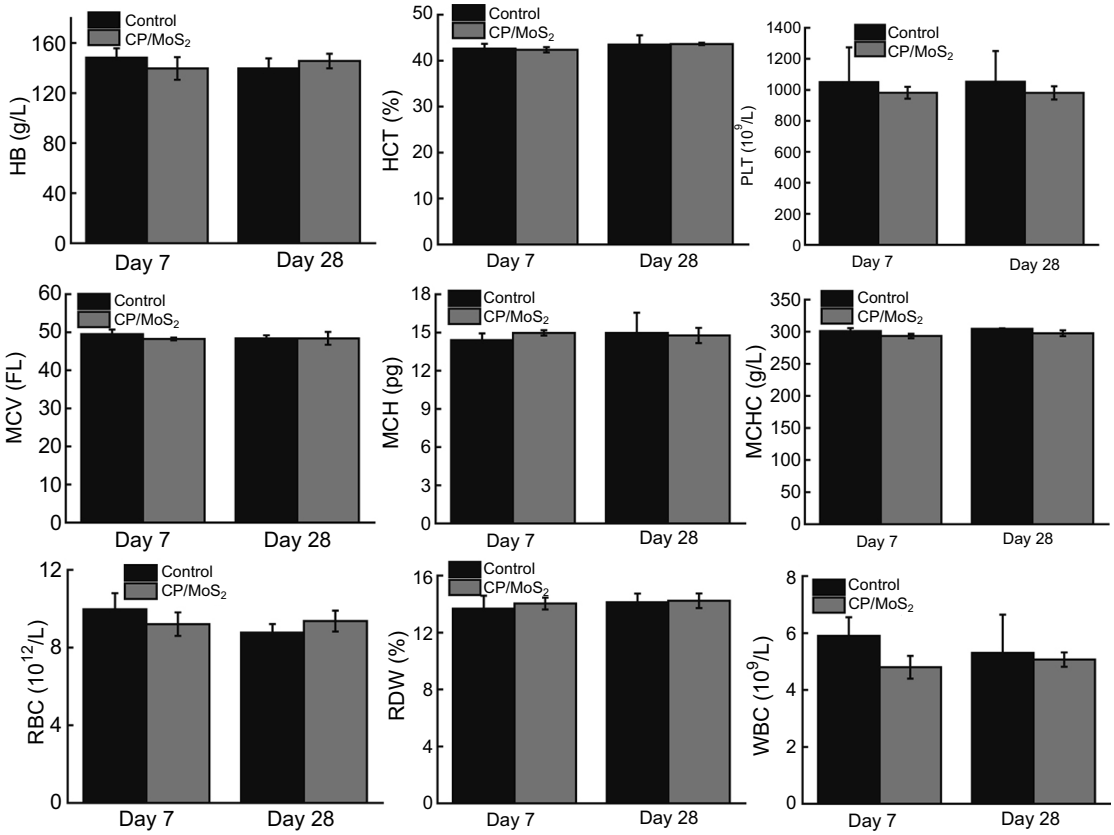

Figure S7 Changes of hemoglobin (HB), hematocrit (HCT), platelet (PLT), mean corpuscular volume (MCV), mean corpuscular hemoglobin (MCH), mean corpuscular hemoglobin concentration (MCHC), red blood cell count (RBC), red cell distribution width (RDW), and white blood cell count (WBC) of healthy Kunming mice (control) and mice treated with CP/MoS_2 nanofibrous mat for 7 and 28 days (mean±SD, n=3).
Abbreviation: CP, chitosan/polyvinyl alcohol.

International Journal of Nanomedicine

Dovepress

Publish your work in this journal

The International Journal of Nanomedicine is an international, peer-reviewed journal focusing on the application of nanotechnology in diagnostics, therapeutics, and drug delivery systems throughout the biomedical field. This journal is indexed on PubMed Central, MedLine, CAS, SciSearch®, Current Contents®/Clinical Medicine, Journal Citation Reports/Science Edition, EMBase, Scopus and the Elsevier Bibliographic databases. The manuscript management system is completely online and includes a very quick and fair peer-review system, which is all easy to use. Visit http://www.dovepress.com/testimonials.php to read real quotes from published authors.

Submit your manuscript here: https://www.dovepress.com/international-journal-of-nanomedicine-journal